JACS
JOURNAL OF THE AMERICAN CHEMICAL SOCIETY
Article
pubs.acs.org/JACS

Systematic and Controllable Negative, Zero, and Positive Thermal Expansion in Cubic $Zr_{1-x}Sn_xMo_2O_8$

Sarah E. Tallentire,[†] Felicity Child,[†] Ian Fall,[†] Liana Vella-Zarb,[†] Ivana Radosavljević Evans,[†] Matthew G. Tucker,[‡] David A. Keen,[‡] Claire Wilson,[§] and John S. O. Evans*[,†]

[†]Department of Chemistry, Durham University, Science Laboratories, South Road, Durham DH1 3LE, United Kingdom

[‡]ISIS Neutron and Muon Source, Science and Technology Facilities Council, Rutherford Appleton Laboratory, Harwell Oxford, Didcot OX11 0QX, United Kingdom

[§]Diamond Light Source, Didcot OX11 0DE, Oxon, United Kingdom

Supporting Information

ABSTRACT: We describe the synthesis and characterization of a family of materials, $Zr_{1-x}Sn_xMo_2O_8$ ($0 < x < 1$), whose isotropic thermal expansion coefficient can be systematically varied from negative to zero to positive values. These materials allow tunable expansion in a single phase as opposed to using a composite system. Linear thermal expansion coefficients, α_l, ranging from $-7.9(2) \times 10^{-6}$ to $+5.9(2) \times 10^{-6}$ K^{-1} (12−500 K) can be achieved across the series; contraction and expansion limits are of the same order of magnitude as the expansion of typical ceramics. We also report the various structures and thermal expansion of "cubic" $SnMo_2O_8$, and we use time- and temperature-dependent diffraction studies to describe a series of phase transitions between different ordered and disordered states of this material.

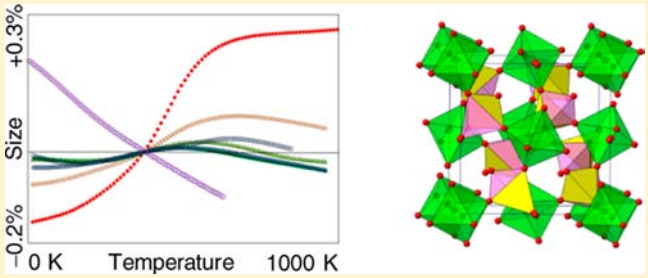

INTRODUCTION

In recent years there has been significant interest in phases that show a bulk contraction in volume on heating, so-called negative thermal expansion (NTE) materials.[1−5] One of the main reasons for this interest is the possibility of using NTE phases in conjunction with normal positive thermal expansion (PTE) phases to produce composites with controllable negative, positive, or even zero thermal expansion (ZTE). Such composites have a range of potential applications where high-precision thermal control is needed. The expansion properties and lifetimes of ZTE composites will, however, depend critically on their microstructure, and the inevitable stresses caused at interfaces between expanding and contracting components can lead to failure. The ability to systematically control the thermal expansion of a single phase over a range of values from NTE to PTE, including ZTE, over a wide temperature range would therefore offer a significant step forward. In this paper we report how such control can be achieved in the isotropic $Zr_{1-x}Sn_xMo_2O_8$ system. We also report the fascinating structural chemistry of $SnMo_2O_8$ that underpins this behavior.

Most materials show positive thermal expansion with linear expansion coefficients typically around $(+5−20) \times 10^{-6}$ K^{-1} for metals and ceramics. PTE can ultimately be traced back to the asymmetric nature of a typical interatomic potential, which leads to bond expansion as higher energy vibrational levels are populated. Mechanisms that can give rise to NTE or ZTE over either narrow or extended temperature ranges include valence state or other electronic transitions (e.g., Sm_3C_{60},[6] $BiNiO_3$,[7] YbGaGe[8,9]), magnetic transitions (e.g., the Invar effect,[10] $Mn_3Cu_{1-x}Ge_xN$,[11] CuO and MnF_2[12]), and crystal field/electronic effects at low temperature.[2] Near-zero thermal expansion has been achieved in antiperovskites such as $Mn_3Cu_{1-x}Sn_xN_{1-\delta}$, where a volume-contracting magnetic phase transition counteracts the underlying positive thermal expansion close to the Néel temperature of the material.[4,13] The effect is, however, restricted to a relatively narrow temperature range.

The most common origin of NTE over a wide temperature range is phonon-related, and a number of materials (framework oxides and cyanides, zeolites, metal−organic frameworks) have been shown to display phonon-driven contraction.[2,14] Here the population of negative-Gruneisen-parameter modes on heating, such as those caused by transverse vibrations of M−O−M linkages, brings the metals of the framework closer together. The ultra-low thermal expansion material TaO_2F [α_l varying from $(-1$ to $+1) \times 10^{-6}$ K^{-1} from 25 to 600 °C] owes its behavior to this mechanism.[15−17]

The best-known NTE oxides are the cubic AM_2O_8 family (A = Zr, Hf; M = Mo, W; Figure 1), members of which show isotropic NTE over a wide temperature range.[18−21] ZrW_2O_8 shows isotropic NTE from 2 to 1070 K with a linear expansion coefficient α_l of -9.0×10^{-6} K^{-1} (0−350 K). All materials with

Received: June 20, 2013
Published: July 29, 2013

   dx.doi.org/10.1021/ja4060564 | J. Am. Chem. Soc. 2013, 135, 12849−12856

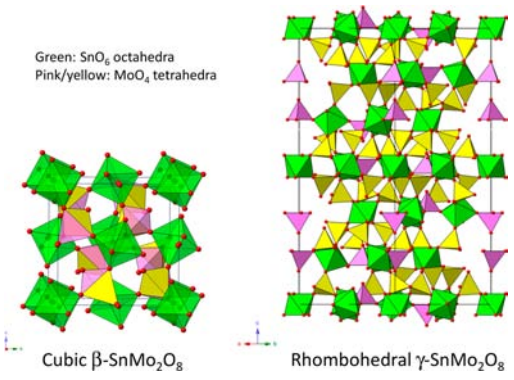

Figure 1. Structures of cubic β-$SnMo_2O_8$ and rhombohedral γ-$SnMo_2O_8$. SnO_6 octahedra are shown in green, and MoO_4 tetrahedra in yellow/pink. At high temperature, β-$SnMo_2O_8$ tetrahedra are dynamically disordered over the yellow/pink sites; the yellow sites are those that would be occupied in ordered $P2_13$ α-ZrW_2O_8. In ordered rhombohedral γ-$SnMo_2O_8$, occupied tetrahedral orientations are shaded as yellow (same) or pink (reversed) to show their orientation relative to those in α-ZrW_2O_8.

the basic topology shown in Figure 1 have been reported to exhibit NTE, and this has been related to the flexible structure of the network of corner-sharing AO_6 octahedra and MO_4 tetrahedra. This topology supports a family of low-energy negative-Gruneisen-parameter modes,[22] which can be described within the (quasi) rigid unit mode (qRUM or RUM) language of Dove and co-workers.[23−25]

There have been many attempts to systematically tune the thermal expansion properties of AM_2O_8 materials via chemical substitution, though these have had limited success. The phase diagrams of the ZrW_2O_8 and $ZrMo_2O_8$ systems are such that the cubic phases are thermodynamically stable only in a narrow temperature window (1378−1530 K for ZrW_2O_8; ∼1400 K for $ZrMo_2O_8$).[26,27] For ZrW_2O_8 the binary oxides are stable at lower temperatures, whereas for $ZrMo_2O_8$ two PTE polymorphs (monoclinic α and trigonal β) are more stable than the cubic form. The synthesis of Mo-containing systems is further complicated by the volatility of MoO_3 at high temperatures, and careful low-temperature precursor-based routes are required for their preparation. With the exception of Hf, substitutions reported to date on the A site show a limited range of solubility: $Zr_{1-x}Sn_xW_2O_8$ ($x \leq 0.2$), $Zr_{1-x}Ti_x$ (≤ 0.05), and $Zr_{1-x}Ln_x$ ($x \leq 0.05$; Ln^{3+} = Sc, Y, In, Eu, Er, Yb, or Lu).[28−36] The thermal contraction properties on substitution are largely unchanged, though the temperature of the α−β phase transition (see below) can be altered, influencing lower-temperature expansion.

Due to synthetic challenges, no significant control of thermal expansion via A-site substitution in the $ZrMo_2O_8$ system has been reported. However, size considerations and the crystal chemistry of related systems suggest that a cubic Sn-substituted system should be at least kinetically stable. The literature relating to the oxygen-rich part of the Sn−O−Mo system is a little confused. A stable (500−903 °C) $SnMo_2O_8$ phase was claimed by early workers,[37] though others have failed to reproduce this, suggesting the sample was a binary oxide mixture.[38,39] There have, however, been two reports of preparation of $SnMo_2O_8$ with a structure related to cubic $ZrMo_2O_8$ via a low-temperature route that involves flowing $SnCl_4$ vapor in an O_2 carrier gas over solid MoO_3.[39,40] Little information has appeared on this material, and neither its physical properties nor its potential influence on NTE systems have been investigated. In this paper we report the development of a reliable and reproducible way to produce phase-pure $SnMo_2O_8$ for the first time, allowing us to determine its complex structural landscape. $SnMo_2O_8$ is remarkable in the cubic AM_2O_8 family in that it has positive thermal expansion. We also report how this development leads to the ability to form a solid solution, $Zr_{1-x}Sn_xMo_2O_8$, which has a completely tunable thermal expansion from positive to negative, including near zero-expansion compositions. We thus reveal an unprecedented level of chemical control of thermal expansion (NTE, ZTE, PTE) in a single phase over a very wide temperature range.

EXPERIMENTAL SECTION

Synthesis. α-$SnMo_2O_8$ was prepared by two routes. Using the method of Buiten,[40] we could prepare the phase over the temperature range 773−873 K with up to 90% pure samples (impurities ∼5% SnO_2, ∼5% MoO_3) formed after 7 h of heating at 773 K. Cubic materials $Zr_{1-x}Sn_xMo_2O_8$ over the range $0.2 \leq x \leq 1$ were also prepared by a coprecipitation route, followed by controlled annealing of the amorphous product. In a typical synthesis ($x = 0.5$), 1.0522 g of $SnCl_4{\cdot}5H_2O$ (3.0 mmol, 98%, Aldrich) and 0.9660 g of $ZrOCl_2{\cdot}8H_2O$ (3.0 mmol, 98%, Aldrich) were dissolved in 12 cm^3 of distilled water to form a colorless solution. $(NH_4)_6Mo_7O_{24}{\cdot}4.89H_2O$ (2.1374 g, 1.71 mmol, 99.999%, Alfa Aesar) was dissolved in 12 cm^3 of distilled water to form a colorless solution. The two solutions were added alternately dropwise to 6 cm^3 of distilled water with continuous stirring. A purple/gray precipitate formed immediately and the suspension was stirred overnight. The precipitate was dried in an oven at 323 K to obtain a lilac amorphous solid. Pale yellow crystalline cubic $Zr_{1-x}Sn_xMo_2O_8$ was obtained by heating at 2 K/min to 853 K and holding for 0.5 h.

Powder Diffraction. Variable-temperature diffraction data were collected in Bragg−Brentano geometry on a Bruker d8 diffractometer equipped with a LynxEye linear position-sensitive detector using Cu $K\alpha_{1/2}$ radiation. High-temperature data were collected by use of an Anton-Paar HTK1200 environmental heating chamber. Temperature calibration was checked with an Al_2O_3 internal standard following a published protocol.[41] Low-temperature data were collected on an Oxford Cryosystems pHeniX cryostat. Quench-hold diffraction data of Figure 4 were collected on a sample mounted in a 0.3 mm capillary and recorded in transmission mode on a Bruker d8 diffractometer fitted with a parallel-beam Göbel mirror. The sample was cooled by use of an Oxford Cryosystems cobra cryostream, and temperature calibration was confirmed by use of an external standard.

For the in situ data collected during sample synthesis in Figure 3b (and similar experiments for $0.2 \leq x \leq 1.0$), quantitative Rietveld refinement was performed with the seven different crystalline phases that were observed during synthesis of the whole $Zr_{1-x}Sn_xMo_2O_8$ series. The amount of amorphous material was estimated by mixing 25% (by mass) crystalline Al_2O_3 with each sample. Due to the absorption difference between the standard and other phases, a Brindley correction was applied during refinement. An appropriate value for the correction (corresponding to 4 μm particles) was determined by analyzing a known mixture of Al_2O_3, ZrO_2, and MoO_3. Due to reactivity with components, we could not use standards with a closer absorption coefficient.

All Rietveld refinements were performed with the Topas Academic software suite. Selected refinement results are given in the figure captions and main text. Full crystallographic details are given in Supporting Information.

RESULTS AND DISCUSSION

Thermal Expansion of Cubic $SnMo_2O_8$. Powder diffraction of a sample of cubic $SnMo_2O_8$ prepared by the method of Buiten[40] confirmed that the structure was closely related to cubic $ZrMo_2O_8$ (see Figure S1 in Supporting

dx.doi.org/10.1021/ja4060564 | J. Am. Chem. Soc. 2013, 135, 12849−12856

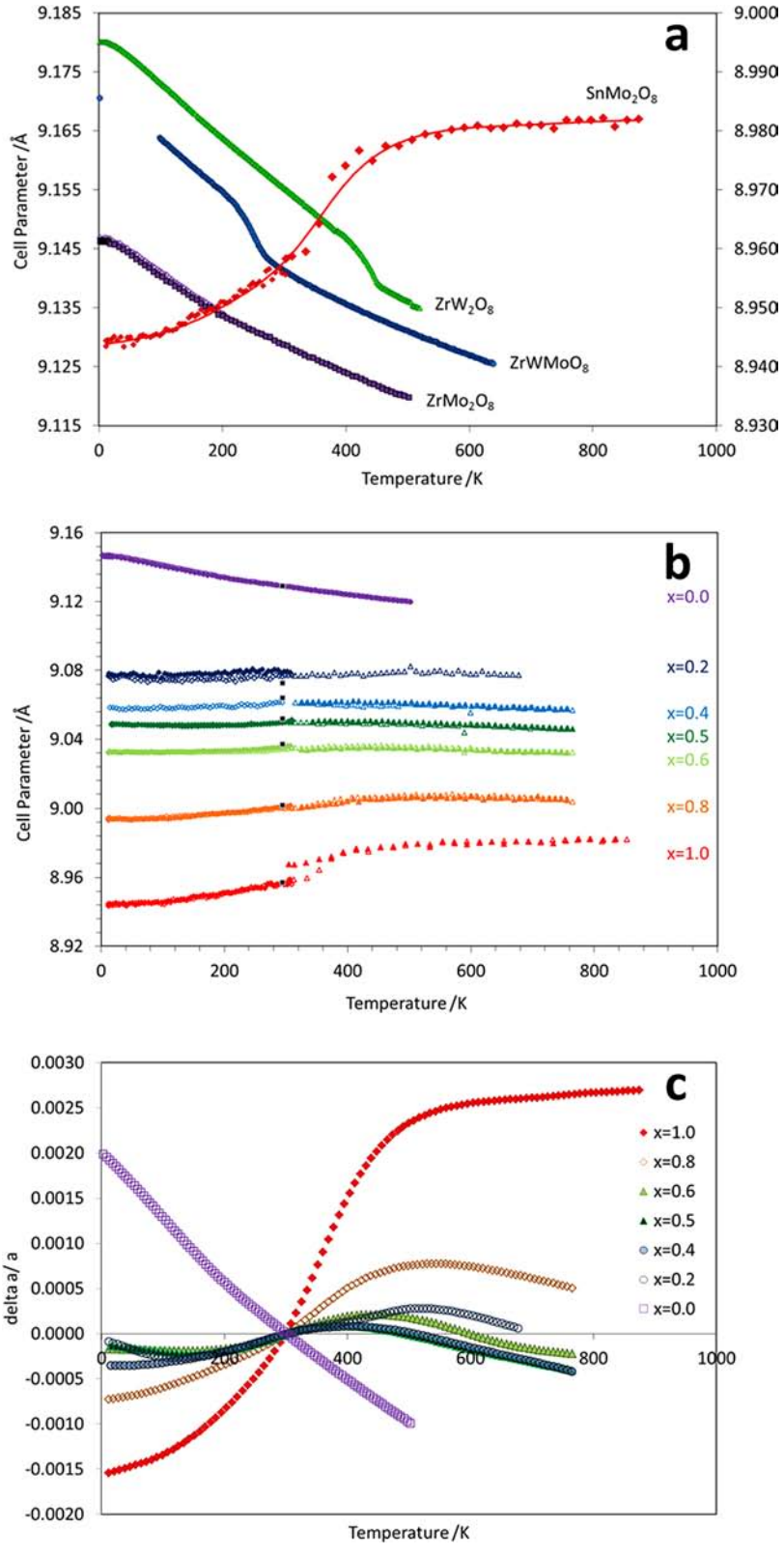

Figure 2. Thermal expansion of $Zr_{1-x}Sn_xMo_2O_8$. (a) Unit cell parameters for cubic ZrW_2O_8, $ZrWMoO_8$, and $ZrMo_2O_8$ (left-hand axis) and α/β-$SnMo_2O_8$ (right-hand axis). (b) Cell parameters extracted from powder diffraction data collected on warming (open symbols) and cooling (solid symbols) $Zr_{1-x}Sn_xMo_2O_8$ materials in a cryostat (circles) or furnace (triangles). (■) Cell parameters at 300 K, determined by use of a Si internal standard. Small calibration offsets of furnace data have been applied to match 300 K cells (0.0017, 0.005, 0.0036, 0.0027, 0.0019, and 0.0044 Å for x = 0.2, 0.4, 0.5, 0.6, 0.8, and 1.0, respectively). (c) Thermal expansion data in the form $(a_T - a_{300K})/a_{300K}$ for $Zr_{1-x}Sn_xMo_2O_8$ materials derived from spline fitting of data in panel b.

dx.doi.org/10.1021/ja4060564 | J. Am. Chem. Soc. 2013, 135, 12849−12856

Information and Figure 5b). We call the room-temperature form of this material α-$SnMo_2O_8$. The thermal expansion of α-$SnMo_2O_8$ is shown in Figure 2a in comparison to other AM_2O_8 materials. α-$SnMo_2O_8$ is unique among cubic AM_2O_8 systems in that it shows a positive expansion coefficient: α_l is $+1.0 \times 10^{-5}$ K^{-1} from −100 to +100 °C, compared to -7.8×10^{-6} K^{-1} for α-ZrW_2O_8 over the same range. From around 330 K, α-$SnMo_2O_8$ undergoes a volume-increasing ($\Delta V \sim +0.6\%$) phase transition. Changes in the powder diffraction pattern through this phase transition are minimal (Figure S2 in Supporting Information), suggesting minimal structural changes. This phase transition is explored in more detail below.

Synthesis and Thermal Expansion of $Zr_{1-x}Sn_xMo_2O_8$. Due to difficulties with reproducibility of the flow synthesis of α-$SnMo_2O_8$ (control of flow rate, reagent surface area, MoO_3 and $Mo_2O_2Cl_2$ volatility, ubiquitous presence of impurities, etc.), we have developed an alternate low-temperature synthesis. Initially a precursor is formed via coprecipitation of $SnCl_4 \cdot 5H_2O$ and $(NH_4)_6Mo_7O_4 \cdot 5H_2O$ solutions to form an amorphous $SnMo_2O_y(OH)_{16-2-y} \cdot nH_2O$ material. Heating this material to 863 K for 0.5 h led to a high-purity sample of α-$SnMo_2O_8$. By replacing appropriate amounts of $SnCl_4 \cdot 5H_2O$ by $ZrOCl_2 \cdot 8H_2O$, we have been able to prepare cubic materials $Zr_{1-x}Sn_xMo_2O_8$ over the range $0.2 \le x \le 1$ by this route. This A-site solubility range is significantly higher than has been possible in other AM_2O_8 systems. Sample structure and composition have been determined by powder diffraction and energy-dispersive X-ray spectroscopy (EDX) on selected samples. Materials with $x < 1$ are typically slightly Sn-deficient, which can be compensated by use of a small excess of Sn during synthesis. Accurate cell parameters for the cubic phases have been determined by use of a Si internal standard and are included in Figure 2b and in Supporting Information. For Zr-rich samples ($x < \sim 0.4$), preparation of the cubic phase becomes progressively more difficult due to increased competition with the formation of trigonal phases. This is unsurprising given the literature on $ZrMo_2O_8$ and the importance of proceeding via the so-called LT intermediate phase in accessing cubic γ-$ZrMo_2O_8$.[42−44]

Optimum kinetically controlled synthetic conditions for accessing these metastable AM_2O_8 materials have therefore been determined by in situ X-ray diffraction studies. Figure 3a shows a typical experiment in which a series of diffraction patterns were recorded upon warming a sample of amorphous $Zr_{0.4}Sn_{0.6}Mo_2O_y(OH)_{16-2-y} \cdot nH_2O$ from room temperature to 1120 K. Crystalline Al_2O_3 (25% by mass) was mixed with the sample as an inert internal standard to allow quantification of the amorphous content on heating. Figure 3b shows the quantitative phase analysis. From room temperature to ~670 K, the sample remains amorphous. Between ~670 and 720 K, cubic $Zr_{0.4}Sn_{0.6}Mo_2O_8$ forms as the only crystalline phase. The amorphous content falls to close to 0 within the precision of the experiment, indicating that crystalline $Zr_{0.4}Sn_{0.6}Mo_2O_8$ is the principal phase present. No intermediate crystalline phases, such as the LT phase observed in the $ZrMo_2O_8$ system, are seen. Above ~1000 K, cubic $Zr_{0.4}Sn_{0.6}Mo_2O_8$ decomposes, SnO_2 and ZrO_2 related phases are formed, and MoO_3 is lost by volatilization. MoO_3 loss is consistent with ex situ studies of the synthesis of tin molybdenum oxides and explains the apparent rise in amorphous content at high temperatures.[38] Similar behavior is observed for samples with $0.5 \le x \le 1$. For $0.2 \le x \le 0.5$, the cubic material can be formed as the major crystalline phase (up to ~85% cubic/15% trigonal at $x = 0.2$), though

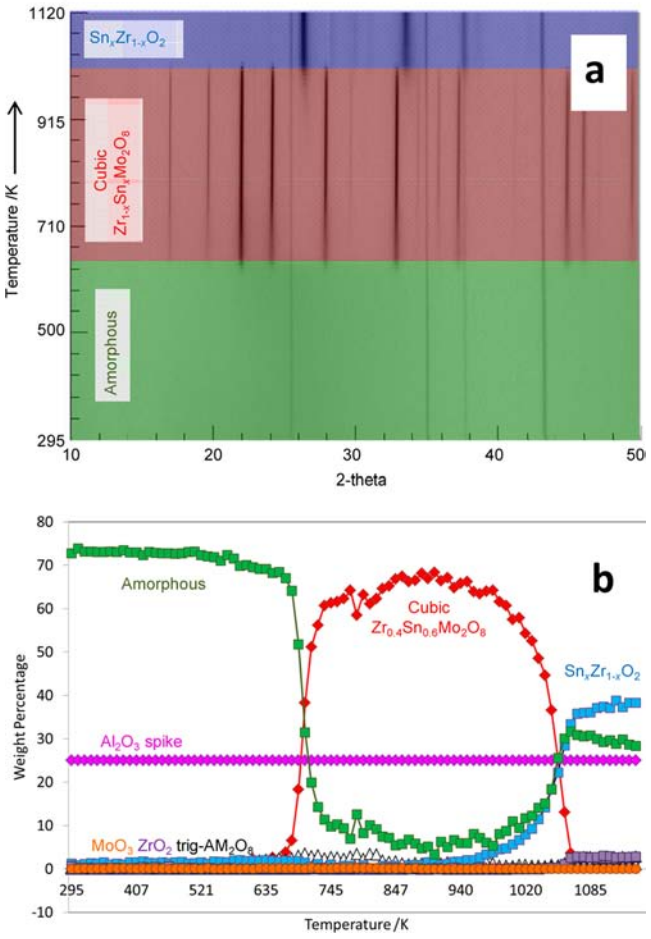

Figure 3. In situ diffraction study of $Zr_{0.4}Sn_{0.6}Mo_2O_8$ synthesis. (a) Surface plot of powder diffraction on warming amorphous $Zr_{0.4}Sn_{0.6}Mo_2O_y(OH)_{16-2-y} \cdot nH_2O$ mixed with 25% by weight Al_2O_3 internal standard from room temperature to 1120 K. (b) Phase quantification by Rietveld refinement.

some amorphous component (10−20%) may still be present. Cell parameters of the cubic phase (see Figure S3 in Supporting Information) suggest a full range of solid solution is possible for $0.2 \le x \le 1.0$. Work is underway to try and improve phase purity at the Zr-rich end of the solid solution to allow access to bulk cubic samples over the whole composition range.

Figure 2c shows thermal expansion data of a series of samples for $0 \le x \le 1$ in the form of $\Delta a/a_{300K}$. The thermal expansion of this system can be systematically controlled over the range $\alpha_l = [-5.9(2)$ to $+7.9(2)] \times 10^{-6}$ K^{-1} (12−500 K). Systems with approximately equal Sn:Zr ratios have extremely low coefficients of expansion over the entire temperature range studied, with $Zr_{0.4}Sn_{0.6}Mo_2O_8$ having essentially zero thermal expansion from 12 to 600 K [$\alpha_{12-600} = -6(20) \times 10^{-8}$ K^{-1}].

This level of control of thermal expansion and contraction within a single cubic phase over such a wide temperature range is unprecedented. Previous studies on expansion control in materials such as $ZrV_{2-x}P_xO_7$ have involved systems where end members both show positive thermal expansion close to room temperature, and low/negative expansion is achieved only at significantly higher temperatures.[45]

Temperature- and Time-Dependent Structural Phase Transitions in Cubic $SnMo_2O_8$. In addition to its role in allowing us to produce near-ZTE in cubic AM_2O_8 materials, the

dx.doi.org/10.1021/ja4060564 | J. Am. Chem. Soc. 2013, 135, 12849−12856

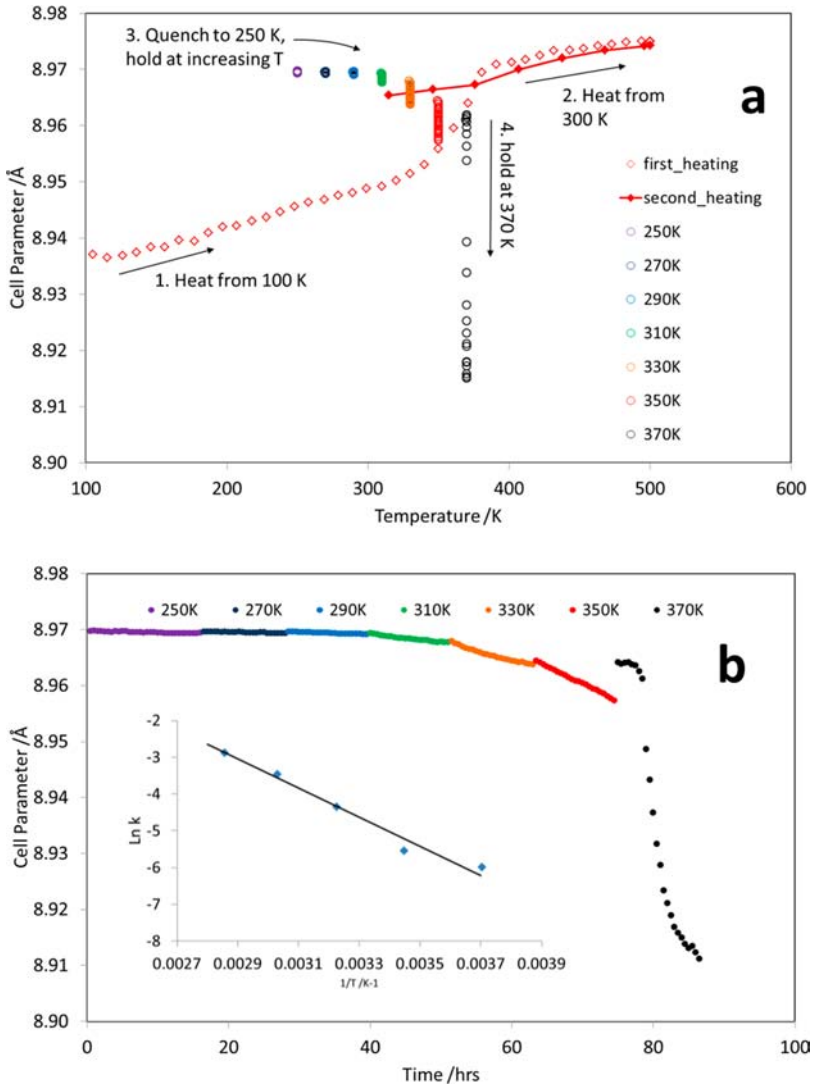

Figure 4. Oxygen ordering in $SnMo_2O_8$. (a) Cell parameter evolution upon (1) heating α-$SnMo_2O_8$ from 100 to 500 K at 20 K/h, (2) cooling to room temperature and then heating to 500 at 60 K/h, (3) quenching from 500 to 250 K and then holding isothermally at increasing temperatures for 12 h periods, up to (4) 370 K. (b) Cell parameters from stage 3 of panel a, plotted as a function of experimental time; inset shows Arrhenius plot. Data were collected on a sample mounted in a 0.3 mm capillary on a Bruker d8 diffractometer operating in transmission mode with Cu $K\alpha_{1/2}$ radiation.

$x = 1$ α-$SnMo_2O_8$ material shows unexpected changes as a function of time and temperature, which reveal new aspects of the structural chemistry of this important family. First, thermal expansion studies on α-$SnMo_2O_8$ reveal a volume-increasing phase transition between ~330 and 390 K; we call the high-temperature phase the β form. This behavior is again in contrast to other AM_2O_8 systems, where heating over similar temperatures can lead to volume-decreasing phase transitions that are associated with a dynamic order−disorder phase transition of the orientation of pairs of 2 × MO_4 tetrahedra along the cubic ⟨111⟩ direction (see Figure 1a). In ZrW_2O_8 this changes the symmetry from noncentrosymmetric $P2_13$ in the ordered α form to centrosymmetric $Pa\bar{3}$ in the disordered β form.[46] Similar though less pronounced transitions are seen for $Zr_{1-x}Sn_xMo_2O_8$ with $x < 1$.

Repeated thermal expansion measurements on warming and cooling $SnMo_2O_8$ through the α to β phase transition showed that freshly prepared samples all had thermal expansion similar in form to Figure 2a, but unusually large differences were observed between room-temperature cell parameters depending on the sample's thermal history (see Figure S4 in Supporting Information). Cell parameters of samples held for extended periods at room temperature also often showed a small but measurable decrease in cell parameter over time (see Figure S7 in Supporting Information). This contraction occurred for samples sealed in glass capillaries and also for samples held under a dynamic vacuum of 10^{-4} atm, suggesting that it was not caused by water uptake as has been observed in other members of the AM_2O_8 family.[47,48] This observation suggested that α-$SnMo_2O_8$ could exist in a kinetically trapped glassy state related to the high-temperature dynamically disordered form.

Figure 4 shows the results of a series of time- and temperature-dependent diffraction experiments designed to probe this behavior. A sample of α-$SnMo_2O_8$ was heated from 300 to 500 K, quench-cooled in liquid nitrogen (<30 s to cool from 500 to 100 K), and then held for 12 h periods at seven temperatures between 250 and 370 K; powder data were recorded in multiple 30 min time slices at each temperature. Figure 4a shows all the cell parameters determined, plotted as a

dx.doi.org/10.1021/ja4060564 | J. Am. Chem. Soc. 2013, 135, 12849−12856

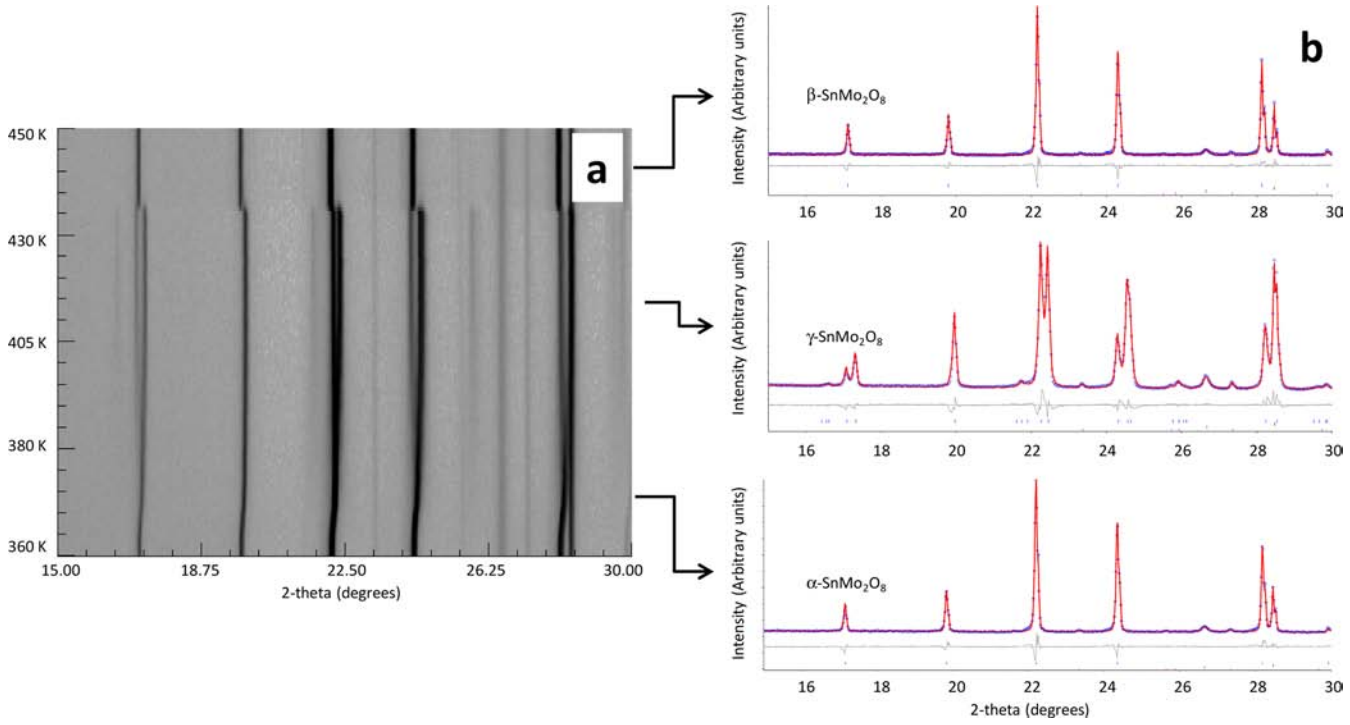

Figure 5. (a) Surface plot of powder diffraction data of $SnMo_2O_8$ held for 6 h as temperature increased in 10 K intervals from 360 to 450 K. (b) Rietveld refinements of the α, cubic β, and rhombohedral γ structures. γ refinement was performed on data collected on a sample cooled back to room temperature. A Si internal standard (lower tick marks) was used. Observed data are shown in blue, calculated in red, and differences in gray. Small vertical bars show positions of allowed *hkl* reflections. Data were collected with Cu $K\alpha_{1/2}$ radiation in reflection mode.

function of temperature. The time-zero 250 K cell parameter (8.9698 Å) suggests that quench-cooling is able to freeze in the high-temperature form. Figure 4b (which shows the same data as a function of time) shows that there is then a small but significant reduction in cell parameter as the sample is held at constant temperature. Upon stepping the temperature to 270 K, there is an initial increase in cell parameter (normal positive thermal expansion) followed by a further decrease during the isothermal treatment. The rate of contraction of $SnMo_2O_8$ with time increases significantly with increasing temperature as expected for an activated process. A simple Arrhenius treatment assuming evolution to a constant state yields an apparent activation energy of 33(2) kJ·mol^{-1} for data from 270 to 350 K. This compares with E_A values for oxygen migration via polyhedral rearrangement in ZrW_2O_8 from solid-state ^{17}O NMR of 24.5(5) kJ·mol^{-1} in α-ZrW_2O_8, 42(9) kJ·mol^{-1} in β-ZrW_2O_8,[21,49] and 34(5) kJ·mol^{-1} in $ZrWMoO_8$.[21]

The data in stage 3 of Figure 4a suggested that the cell parameters of a time- and temperature-evolved quench-cooled sample and a normal warmed sample would converge at ~370 K and an equilibrium state would be reached. Initial isothermal data recorded at 370 K suggested this behavior with $a \approx 8.962$ Å (start of stage 4 of Figure 4a). However, a large and rapid reduction in cell parameters ($\Delta V \approx -1.7\%$), accompanied by marked broadening of several peaks in the diffraction pattern, was observed after ~6 h at 370 K. Upon holding the sample at 400 K for 5 h, the broadening evolved into a clear splitting of most reflections in the powder pattern. The peak splitting pattern observed is indicative of a complete phase transition to rhombohedral symmetry with a cell of $a \approx 12.50$ Å and $c \approx 31.10$ Å with $c/2a = 1.244$, a 1.6% distortion from metrically cubic symmetry (transformation [−110; 0−11; 222]).[50] This rhombohedral phase remained stable upon cooling to room temperature. Similar phase evolution was observed in a fresh sample of α-$SnMo_2O_8$ warmed from room temperature. Figure 5a shows a surface plot of powder diffraction data collected for 12 × 30 min at each of 10 temperatures from 360 to 450 K. Clear peak splitting indicative of the phase transition to rhombohedral symmetry is observed at ~390 K, followed by a sharp, first-order transition upon further heating at ~440 K back to the high-temperature β form.

Structural Relationships. The fascinating thermal expansion properties of this system are intimately linked to its complex structural chemistry. Full crystallographic details of the structures and structural relationships between the different forms of $SnMo_2O_8$ encountered will be published elsewhere, and we will restrict discussion here to the gross changes that occur. We will denote the initial low-temperature metrically cubic form as α-$SnMo_2O_8$, the rhombohedral form prepared by annealing at 400 K as γ-$SnMo_2O_8$, and the high-temperature form as β-$SnMo_2O_8$.

Powder neutron and single-crystal X-ray diffraction data show that high-temperature β-$SnMo_2O_8$ is cubic and isostructural with the $Pa\bar{3}$ high-temperature form of β-ZrW_2O_8 or room-temperature γ-$ZrMo_2O_8$ (see Supporting Information). In this form the orientations of pairs of 2 × MoO_4 tetrahedra are dynamically disordered along the cubic ⟨111⟩ axes as shown in Figure 1a. Figure 6 shows that peak intensities in the X-ray powder diffraction patterns of low-temperature α-$SnMo_2O_8$ are very similar to those in the high-temperature β form, indicating a strong similarity in the structures and suggesting that it has a predominantly disordered arrangement of MoO_4 tetrahedra. Single-crystal diffraction data reveal, however, extra reflections over those observed for the simple β structure at high temperature. All observed reflections could be indexed by use of a rhombohedral

dx.doi.org/10.1021/ja4060564 | J. Am. Chem. Soc. 2013, 135, 12849−12856

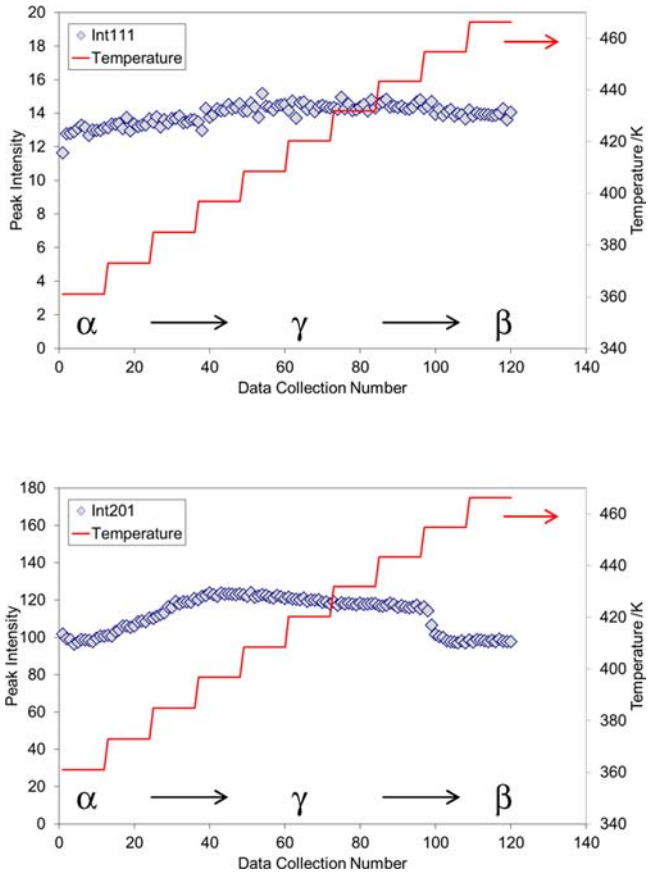

Figure 6. Intensities of representative X-ray peaks as α-$SnMo_2O_8$ is gradually heated from 360 to 460 K, as shown in Figure 5a. Plots show the summed intensities of families of peaks related to individual *hkl* reflections in the cubic β phase. The 111 reflection shows minimal changes with temperature, while 201 (and other peaks; see Supporting Information) show significant intensity changes upon entering the rhombohedral γ phase associated with ordering of 2 × MoO_4 tetrahedra. Peak intensities revert to values similar to those in the α phase on passing through the γ to β transition. Temperature profile is shown on the right-hand scale.

unit cell with a = 12.6 Å and c = 31.0 Å at 120 K, which represents a doubling in the volume relative to the cubic cell, which would have a = 12.6 Å and c = 15.5 Å in this rhombohedral setting. By Rietveld or Pawley fitting of high-resolution laboratory powder diffraction, no metric distortion of the α-$SnMo_2O_8$ cell from cubic symmetry can be observed over its entire stability range [$c/2a$ = 1.2252(3) compared to 1.2247 for undistorted cubic symmetry; see Figure S6 in Supporting Information].

The transition from α- to γ-$SnMo_2O_8$ at ~400 K leads to marked distortion in the cell metric (a = 12.503 Å, c = 31.0958 Å, and $c/2a$ = 1.244, a 1.6% distortion) giving clear peak splitting in the powder pattern and small but observable changes in the integrated intensity of sets of related pseudocubic reflections (e.g., around 10% increase for stronger reflections, a doubling in intensity for the weaker 302 family; see Figure 6). The intensity changes indicate a more marked structural change and powder data of γ-$SnMo_2O_8$ can be fitted well by Rietveld refinement of a model with $R\bar{3}$ symmetry in which the 2 × MoO_4 tetrahedra along the 3-fold axes of the original cubic unit cell adopt an ordered arrangement. Rietveld plots are included in Figure 5b and in Supporting Information. The ordering arrangement differs from that observed in α-ZrW_2O_8 and, by use of a symmetry-adopted distortion mode description,[51] can be described with an R1+R3+ irrep as opposed to the Γ1− irrep that describes ordering in ZrW_2O_8. The different ordering pattern is highlighted in Figure 1. In Figure 1b, the tetrahedral sites occupied in γ-$SnMo_2O_8$ have been shaded as to whether they have the same orientation as in α-ZrW_2O_8 (yellow) or reversed (pink). γ-$SnMo_2O_8$ itself shows positive thermal expansion from 312 to 412 K with $\alpha_l = 1.87 \times 10^{-5}$ K^{-1} and a $c/2a$ ratio that falls smoothly to 1.241 upon heating (Figure S6 in Supporting Information) before transformation to the β form at ~440 K.

Observation of this phase transition to a 2 × MoO_4 ordered structure with a significantly smaller volume than the α or γ forms helps explain the unusual time-dependent behavior observed in cell volumes of Figure 4. The energy landscape of pseudocubic $SnMo_2O_8$ is such that an entropically stabilized dynamically disordered form is stable above ~400 K. At lower temperature, the fully ordered γ form is presumably the thermodynamically stable phase (or at least the locally most stable phase without the extensive reconstruction required for phase segregation or formation of a different polymorph). The rate of MoO_4 reorientation in the structure is sufficiently slow that it is easy to freeze in the high-temperature disorder in the α form, with extremely long time periods required to access the stable γ structure at low temperatures. Partial MoO_4 ordering presumably occurs in α-$SnMo_2O_8$ such that the local structure resembles the lower-volume γ-$SnMo_2O_8$ structure. The unwinding of local cooperative polyhedral tilts would contribute to the PTE of α-$SnMo_2O_8$ at low temperature, and the gradual disruption of local order will cause the volume expansion at the α to β transition. We have treated ZTE $Zr_{1-x}Sn_xMo_2O_8$ with x ~ 0.5 to similar heating regimes as shown in Figure 5a but have not observed transitions to the γ structure.

■ CONCLUSION

$Zr_{1-x}Sn_xMo_2O_8$ is a fascinating system that shows a number of surprises. First, the x = 1 phase is unique among AM_2O_8 materials in showing PTE in all its forms (α, β, and γ). We presume the origin of the PTE arises from a number of contributions. First the 2.6% smaller cell volume relative to ZrW_2O_8 and increased stiffness of smaller SnO_6 octahedra are sufficient that negative-Gruneisen-parameter phonon modes are overwhelmed by positive modes. A general correlation between NTE and cation size has been observed in other systems such as $A_2(MO_4)_3$ and AP_2O_7 materials.[5] There will also be contributions from the unwinding of any cooperative polyhedral tilts allowed in the lower-symmetry α phase and due to the evolution of short-range order of MoO_4 groups. The intrinsic volume and thermal expansion properties of $SnMo_2O_8$ are strongly influenced by the precise pattern of ordering of MoO_4 tetrahedra within the structure, with a range of ordered and disordered configurations accessible close to room temperature. Structural reorientation of the MoO_4 groups occurs from 250 K but becomes sufficiently accessible at 400 K for formation of the ordered γ structure, which has a configuration unique among these materials.

The identification of a PTE phase isostructural to the NTE AM_2O_8 materials has led us to develop a low-temperature route allowing a far greater range of solid solution on the A site of a cubic AM_2O_8 system than has been achieved before. We can

dx.doi.org/10.1021/ja4060564 | J. Am. Chem. Soc. 2013, 135, 12849−12856

thereby systematically control isotropic expansion properties of $Zr_{1-x}Sn_xMo_2O_8$ from positive to negative values, including zero.

■ ASSOCIATED CONTENT

Supporting Information

Seven figures and two tables with full details on Rietveld refinement of neutron diffraction data for β-$SnMo_2O_8$, data similar to Figure 6 for more reflections during α to β to γ transition, Vegard's law plots of cell dependence on x for $Zr_{1-x}Sn_xMo_2O_8$ samples, temperature dependence of cell parameters for $SnMo_2O_8$ samples with a variety of thermal histories, details of Rietveld refinement for γ-$SnMo_2O_8$, and information on variation in cell parameters and $c/2a$ ratio as samples are cycled through α to γ to β to α phase transitions. This material is available free of charge via the Internet at http://pubs.acs.org.

■ AUTHOR INFORMATION

Corresponding Author

john.evans@durham.ac.uk

Notes

The authors declare no competing financial interest.

■ ACKNOWLEDGMENTS

We thank STFC for access to the ISIS facility for neutron scattering experiments and the Diamond Light Source for single-crystal experiments. We thank the EPSRC and Durham University for provision of equipment underpinning the work reported.

■ REFERENCES

(1) Sleight, A. W. *Inorg. Chem.* **1998**, *37*, 2854.
(2) Barrera, G. D.; Bruno, J. A. O.; Barron, T. H. K.; Allan, N. L. *J. Phys.: Condens. Matter* **2005**, *17*, R217.
(3) Evans, J. S. O. *J. Chem. Soc., Dalton Trans.* **1999**, 3317.
(4) Takenaka, K. *Sci. Technol. Adv. Mater.* **2012**, *13*, No. 013001.
(5) Lind, C. *Materials* **2012**, *5*, 1125.
(6) Arvanitidis, J.; Papagelis, K.; Margadonna, S.; Prassides, K.; Fitch, A. N. *Nature* **2003**, *425*, 599.
(7) Azuma, M.; Chen, W.-t.; Seki, H.; Czapski, M.; Olga, S.; Oka, K.; Mizumaki, M.; Watanuki, T.; Ishimatsu, N.; Kawamura, N.; Ishiwata, S.; Tucker, M. G.; Shimakawa, Y.; Attfield, J. P. *Nat. Commun.* **2011**, *2*, No. 347.
(8) Margadonna, S.; Prassides, K.; Fitch, A. N.; Salvador, J. R.; Kanatzidis, M. G. *J. Am. Chem. Soc.* **2004**, *126*, 4498.
(9) Salvador, J. R.; Gu, F.; Hogan, T.; Kanatzidis, M. G. *Nature* **2003**, *425*, 702.
(10) Guillaume, C. E. *C. R. Acad. Sci* **1897**, *125*, 235.
(11) Takenaka, K.; Takagi, H. *Appl. Phys. Lett.* **2005**, *87*, No. 261902.
(12) Zheng, X. G.; Kubozono, H.; Yamada, H.; Kato, K.; Ishiwata, Y.; Xu, C. N. *Nat. Nanotechnol.* **2008**, *3*, 724.
(13) Takenaka, K.; Takagi, H. *Appl. Phys. Lett.* **2009**, *94*, No. 131904.
(14) Miller, W.; Smith, C. W.; Mackenzie, D. S.; Evans, K. E. *J. Mater. Sci.* **2009**, *44*, 5441.
(15) Sawhill, S.; Savrun, E. *Ceram. Int.* **2012**, *38*, 1981.
(16) Tao, J. Z.; Sleight, A. W. *J. Solid State Chem.* **2003**, *173*, 45.
(17) Morelock, C. R.; Greve, B. K.; Cetinkol, M.; Chapman, K. W.; Chupas, P. J.; Wilkinson, A. P. *Chem. Mater.* **2013**, *25*, 1900.
(18) Mary, T. A.; Evans, J. S. O.; Vogt, T.; Sleight, A. W. *Science* **1996**, *272*, 90.
(19) Evans, J. S. O.; Mary, T. A.; Vogt, T.; Subramanian, M. A.; Sleight, A. W. *Chem. Mater.* **1996**, *8*, 2809.
(20) Allen, S.; Evans, J. S. O. *Phys. Rev. B* **2003**, *68*, No. 134101.
(21) Allen, S.; Evans, J. S. O. *J. Mater. Chem.* **2004**, *14*, 151.
(22) The Gruneisen parameter is defined as $d(\ln \nu)/dV$, where ν is the vibrational frequency.
(23) Heine, V.; Welche, P. R. L.; Dove, M. T. *J. Am. Ceram. Soc.* **1999**, *82*, 1793.
(24) Pryde, A. K. A.; Hammonds, K. D.; Dove, M. T.; Heine, V.; Gale, J. D.; Warren, M. C. *J. Phys.: Condens. Matter* **1996**, *8*, 10973.
(25) Tucker, M. G.; Keen, D. A.; Evans, J. S. O.; Dove, M. T. *J. Phys.: Condens. Matter* **2007**, *19*, No. 335215.
(26) Chang, L. L. Y.; Scroger, M. G.; Phillips, B. *J. Am. Ceram. Soc.* **1967**, *50*, 211.
(27) Readman, J. E.; Lister, S. E.; Peters, L.; Wright, J.; Evans, J. S. O. *J. Am. Chem. Soc.* **2009**, *131*, 17560.
(28) De Buysser, K.; Van Driessche, I.; Putte, B. V.; Schaubroeck, J.; Hoste, S. *J. Solid State Chem.* **2007**, *180*, 2310.
(29) De Meyer, C.; Bouree, F.; Evans, J. S. O.; De Buysser, K.; Bruneel, E.; Van Driessche, I.; Hoste, S. *J. Mater. Chem.* **2004**, *14*, 2988.
(30) Guo, F.-L.; Ma, H.; Yang, X.-J.; Deng, X.-B.; Zhao, X.-H. *Chin. J. Inorg. Chem.* **2011**, *27*, 2061.
(31) Hashimoto, T.; Kuwahara, J.; Yoshida, T.; Nashimoto, M.; Takahashi, Y.; Takahashi, K.; Morito, Y. *Solid State Commun.* **2004**, *131*, 217.
(32) Li, H.-H.; Han, J.-S.; Ma, H.; Huang, L.; Zhao, X.-H. *J. Solid State Chem.* **2007**, *180*, 852.
(33) Nakajima, N.; Yamamura, Y.; Tsuji, T. *J. Therm. Anal. Calorim.* **2002**, *70*, 337.
(34) Nakajima, N.; Yamamura, Y.; Tsuji, T. *Solid State Commun.* **2003**, *128*, 193.
(35) Yamamura, Y.; Nakajima, N.; Tsuji, T.; Kojima, A.; Kuroiwa, Y.; Sawada, A.; Aoyagi, S.; Kasatani, H. *Phys. Rev. B* **2004**, *70*, No. 104107.
(36) Yamamura, Y.; Kato, M.; Tsuji, T. *Thermochim. Acta* **2005**, *431*, 24.
(37) Safonov, V. V.; Porotnikov, N. V.; Chaban, N. G. *Zh. Neorg. Khim.* **1983**, *28*, 811.
(38) Berry, F. J.; Hallett, C. *Inorg. Chim. Acta* **1985**, *98*, 135.
(39) Feja, S. Technischen Universitat Dresden, 2004.
(40) Buiten, J. *Polyhedron* **1988**, *7*, 585.
(41) Stinton, G. W.; Evans, J. S. O. *J. Appl. Crystallogr.* **2007**, *40*, 87.
(42) Lind, C.; Wilkinson, A. P.; Hu, Z. B.; Short, S.; Jorgensen, J. D. *Chem. Mater.* **1998**, *10*, 2335.
(43) Lind, C.; Wilkinson, A. P.; Rawn, C. J.; Payzant, E. A. *J. Mater. Chem.* **2001**, *11*, 3354.
(44) Allen, S.; Warmingham, N. R.; Gover, R. K. B.; Evans, J. S. O. *Chem. Mater.* **2003**, *15*, 3406.
(45) Korthuis, V.; Khosrovani, N.; Sleight, A. W.; Roberts, N.; Dupree, R.; Warren, W. W. *Chem. Mater.* **1995**, *7*, 412.
(46) Evans, J. S. O.; David, W. I. F.; Sleight, A. W. *Acta Crystallogr., Sect. B: Struct. Sci.* **1999**, *55*, 333.
(47) Banek, N. A.; Baiz, H. I.; Latigo, A.; Lind, C. *J. Am. Chem. Soc.* **2010**, *132*, 8278.
(48) Duan, N.; Kameswari, U.; Sleight, A. W. *J. Am. Chem. Soc.* **1999**, *121*, 10432.
(49) Hampson, M. R.; Evans, J. S. O.; Hodgkinson, P. *J. Am. Chem. Soc.* **2005**, *127*, 15175.
(50) A metrically cubic rhombohedral cell in hexagonal setting has a c/a ratio of $(3/2)^{0.5}$, giving a $c/2a$ ratio of 1.225 for a cell metrically undistorted from cubic but with the cell volume observed here.
(51) Campbell, B. J.; Stokes, H. T.; Tanner, D. E.; Hatch, D. M. *J. Appl. Crystallogr.* **2006**, *39*, 607.